High sensitivity refractive index sensor based on simple diffraction from phase grating

High sensitivity refractive index sensor based on simple diffraction from phase grating

PANKAJ K SAHOO,[1] JOBY JOSEPH,[1,*] RYOJI YUKINO,[2] ADARSH SANDHU[3]

[1]*Photonics Research Lab, Department of Physics, Indian Institute of Technology Delhi, New Delhi, 110016, India.*

[2]*Electronics-Inspired Interdisciplinary Research Institute (EIIRIS), Toyohashi University of Technology, 1-1 Hibarigaoka, Tempaku, Toyohashi, Aichi 441-8580, Japan.*

[3] *Department of Engineering Science, Graduate School of Information and Engineering, University of Electro-Communications, Tokyo, 1-5-1 Chofugaoka, Chofu, Tokyo 182-8585, Japan.*

Corresponding author: joby@physics.iitd.ac.in

We present a technique for refractive index sensing using a phase grating structure. A grating under normal incidence can be designed such that the 1st order diffracted light travels at a diffraction angle of 90º with respect to the 0th order. The diffracted light which is along the direction of periodicity can further get diffracted from the grating and interfere with the 0th order light. Under this condition, the π phase difference that arises between the two interfering beams results in a transmission dip. We can tune this dip wavelength for senor applications, based on the grating equation. Both simulation and experimental data are presented in the paper which shows good agreement with each other.

OCIS codes: (280.4788) Optical sensing and sensors, (050.1950) Diffraction gratings.

http://dx.doi.org/10.1364/OL.99.099999

Refractive index (r.i.) sensing is widely accepted as an efficient technique for sensing gases, liquids & biomolecules. Various techniques have been proposed for r.i. sensing using metals, dielectrics and semiconductors. One of the most commonly used method is based on the interaction of evanescent field (EF) of electromagnetic field with the sensing medium. Surface Plasmon Resonance (SPR) technique uses the EF of propagating surface plasmon (sp) polaritons at a continuous metal-dielectric interface [1]. Owing to the resonant photon-sp coupling conditions, these sensors are extremely sensitive to r.i. change at the interface. But SPR-sensors are bulkier as they require in general a prism for exciting plasmons. They are also not always suitable for sensing in some selective chemical and bio-chemical nano-architectures [2]. Localized surface plasmon resonance (LSPR) [3] sensors in metallic nanostructures seem much more suitable for this purpose. In addition they are comparatively more miniaturized than SPR. But the sensitivity of LSPR does not exceed 200-500 nm per RIU [4-8]. Also these metal based sensors suffer intrinsic losses which degrades their performance. Instead of metals, this EF sensing method is also used in planar dielectric and semiconductor waveguides [9]. Here the change in effective index (n_{eff}) of a guided mode is measured in response to surrounding r.i. change. These waveguide based EF sensors also require separate coupling units like prism or optical fiber to excite guided modes in the waveguide. There are also alternative EF sensing methods, where such coupling methods are not required, e.g. guided mode resonance (GMR) sensor [10]. GMR sensors use sub wavelength grating on top of a waveguide and they together form the sensing unit. In GMR, one of the diffraction order excites a waveguide mode that couples out and interfere with the 0th order to form transmission (/reflection) dip (/peak). The GMR resonance wavelength gets tuned by changing the r.i. of surrounding medium. The sensitivity of GMR-sensor is in the range 100-300 nm per RIU [11-14].

In this article we report a new planar phase grating based technique for sensing r.i. changes, capable of achieving very high sensitivity compared to other planar EF-based sensors like LSPR & GMR. The sensor geometry consists of a 1D binary phase grating (Fig. 1(a)) over a substrate. The working principle of this new sensor is based on the selective tuning of diffraction from this 1D phase grating. The

periodicity of the grating is Λ_x. Consider a plane wave of wavelength λ with its electric field vector parallel to the grating lines (i.e. along y-direction) incident on the grating from substrate side. For $\lambda < \Lambda_x$, the grating will diffract the incident light into different diffraction orders. The grating equation [15] that predicts the angle of propagation θ_m of the mth order diffracted light is given by equation (1).

$$n \sin \theta_m = n_{inc} \sin \theta_{inc} - m \frac{\lambda}{\Lambda_x} \qquad (1)$$

Here n_{inc} & n are r.i. of the incident (substrate) and the transmitting (cover) medium respectively. θ_{inc} is the angle of incidence in the incident medium. The grating period is chosen such that, after diffraction, 0th order (T_0) propagates in the cover region and the 1st order (D_1 of wavelength λ) propagates at an angle $\theta_m = 90°$. In that case, equation (1) for normal incidence ($\theta_{inc}=0°$) _becomes

$$\lambda = n\Lambda_x \qquad (2)$$

It can be inferred from equation (2) that, if the grating is illuminated by collimated white light, the wavelength, which satisfies eq. (2), is a function of both n & Λ_x. For a fixed period of grating, we can tune λ by changing the r.i. (n). Thus, considering λ as the sensing wavelength, this phase grating can be used as a sensor to sense r.i. of the cover region.
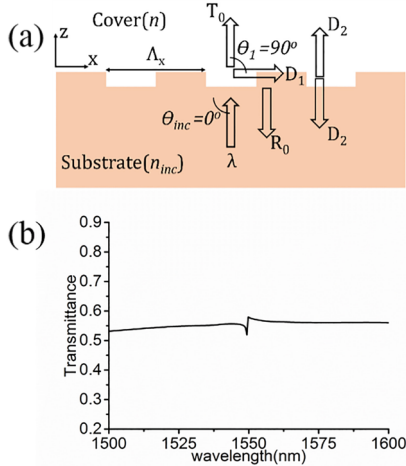

FIG. 1. (a) Diffraction from a phase grating. (b) Transmission dip at 1550nm is obtained due to destructive interference between T_0 & D_2.

Consider the illumination of the phase grating of Fig. 1(a) with collimated white light. The grating period (Λ_x) and r.i. are 1550nm and 1.45 respectively. The substrate and cover r.i. are n_{inc}=1.45 (glass) and n=1.0 (air) respectively. Thus from equation (2), the sensing wavelength will be at 1550nm. Fig. 1(b) shows the simulated transmission spectrum of this grating structure. (We have used Lumerical's FDTD simulation tool [16] to simulate all the transmission (/reflection) spectrums and electric field profiles that are presented in this paper.) As seen from the figure there is a dip at 1550nm. The reason for the observation of the dip at 1550 nm in the transmission spectrum can be explained as follows. It is known that, after diffraction from a phase grating, the first order has a relative phase shift of $\pi/2$ with respect to 0th order [17-20]. As explained in [20], the emerging wave from a phase grating is a phase modulated wave which consist of the original incident plane wave (0th order) plus a localized disturbance. This localized disturbance is nothing but the diffracted wave (D_1 in Fig. 1(a)) that lags by $\pi/2$ phase with respect to the 0th order. So, D_1 propagates along the grating (in x-direction) with a phase shift of $\pi/2$ with respect to T_0. While propagating through the grating, it gets scattered from the grating and diffracts (D_2 in Fig.1 (a)) into the surrounding cover (and to the substrate region) with an additional phase shift of $\pi/2$ with respect to D_1. That is, T_0 & D_2 now have a total of π phase difference between them and hence they interfere destructively in the cover region. This destructive interference will result in a dip in the transmission spectrum of the structure under broadband illumination, as shown in Fig. 1(b). However, as can be seen from Fig. 1(b), the contrast of the dip is not too high to be observable easily in an experiment.
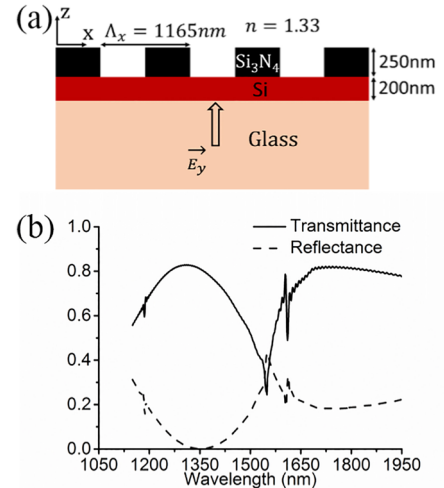

FIG. 2. (a) Sketch of the optimized structure: SiN grating of height 250nm & period 1165nm over a planar Si waveguide of thickness 200nm on glass substrate. (b) Transmission spectrum (solid line) showing dip at 1550nm is obtained due to destructive interference between T_0 & D_2. Also shown in that figure, the reflection spectrum (dashed line) of the sensor.

We optimized our grating parameters to obtain a dip at 1550nm with water (r.i. = 1.33) as reference sensing medium in the cover region. From equation (2), a grating having period 1165 nm immersed in water sets the sensing wavelength λ at 1550nm. We analyzed the transmission spectrum of our structure for different grating parameters such as height and r.i. We also studied the effect of presence of a planar waveguide below the grating layer. We found that, a combined structure of grating and waveguide with proper thickness and r.i. increase the contrast of the dip compared to the case of only grating (without waveguide). While

optimizing our structure, we selected silicon nitride (SiN) and silicon (Si) as materials for grating and waveguide, as these are the most widely used materials. The r.i. of SiN and Si are taken as 2.0 and 3.5 respectively. The final optimized structure is shown in Fig. 2(a). It contains SiN grating of height 250nm over a silicon (Si) planar waveguide of thickness 200nm on top of a glass substrate. The simulated [16] transmission and reflection spectrum for this structure is shown in Fig. 2(b). It shows the formation of a dip in the transmission spectrum and a peak in the reflection spectrum. Similar to the explanation above for a dip, the reason for the formation of peak in the reflection spectrum is because of an additional π phase shift due to the phenomenon of external reflection, which leads to constructive interference between R_0 & D_2 in the substrate region. In the simulation, all material properties like absorption loss and dispersion were taken in to consideration. Even if we don't consider absorption loss and dispersion of materials, the position of the dip is not changed and the spectrum remains almost similar. This indicates that, the cause of above phenomenon is because of phase grating.
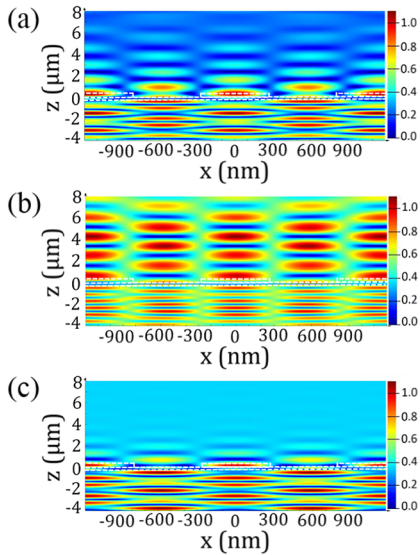

FIG. 3. Electric field profile plotted at three different wavelengths. In (a) at 1550nm, there is destructive interference between T_0 & D_2 in cover region. (b) At 800nm light is diffracted in to the cover region. (c) At 1600nm there is no diffraction, only 0th order propagates in to cover region.

In Fig. 3 we have plotted the electric field profile for three different wavelengths of the transmission spectrum shown in Fig. 2(b). One wavelength corresponding to the dip position at 1550nm is shown in Fig. 3(a). It shows that in the cover region, there is destructive interference. The other two wavelengths shown in figure 3(b) and 3(c) correspond to 800nm and 1800nm respectively. At 800nm wavelength, since $\lambda < \Lambda_x$ light gets diffracted by the grating and propagates in to cover as shown in Figure 3(b). The light corresponding to 1800nm does not get diffracted by the grating as the wavelength is larger than period ($\lambda > \Lambda_x$) of grating. Thus

only the 0th order light propagates in to the cover region as shown in Figure 3 (c).
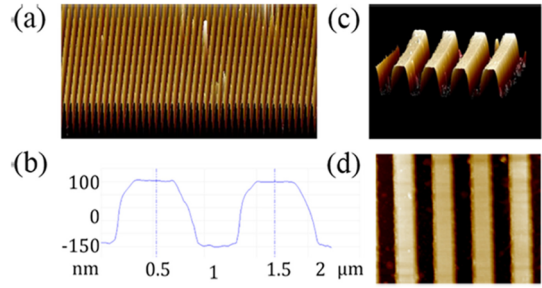

FIG. 4. AFM image of fabricated grating. (a) Large area view, (b) data showing grating height 250 nm and period 1165 nm, (c) perspective view, (d) top view.

For the experimental demonstration of the proposed phase grating sensor, Si (200nm) and SiN (250nm) films were deposited on a quartz plate by sputtering method. Electron beam lithography and RIE was used to transform the SiN film to the required grating structure of period 1165nm and depth 250nm. The grating region is about 5mm x 5mm which gives around 4300 grating lines. This number of grating lines are sufficient to compare it with the infinite number of grating lines in simulation. The AFM image of the fabricated grating is shown in Figure 4.
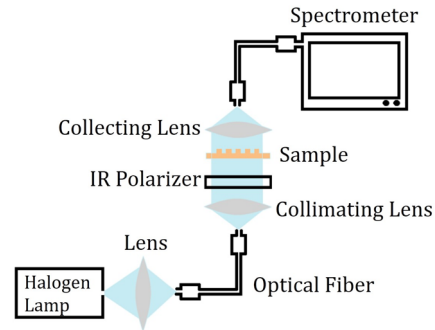

FIG. 5. Schematic of experimental set up to measure transmission spectrum of the sensor. Multimode optical fiber and lens are used for light coupling. An IR polarizer is used to get polarized light whose polarization direction is parallel to grating lines. Lens is used for light collimation.

The transmission spectrum was obtained using optical spectrum analyzer (OSA). The schematic of the experimental set up is shown in Fig. 5. A halogen lamp was used as the broadband light source. Deionized water and sucrose solutions of different concentrations were prepared to check the r.i. sensitivity of the sensor. Abbe refractometer was used to measure the r.i. of the prepared sucrose solutions. The experimentally obtained transmission spectrum is shown in Fig. 6 along with the simulated spectrum result.
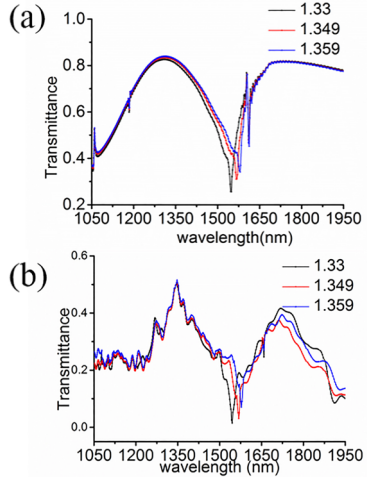
FIG. 6. Graph showing shifting of transmission dip with change in refracting index of cover region: (a) Simulation, (b) Experiment.

The sensitivity (S) of a sensor is defined as the shift in wavelength per unit r.i. change of the sensing medium. In Fig. 6 we have shown the transmission spectrum for three different r.i. of the sensing medium. The Abbe refractometer measured r.i. of the sensing medium are 1.33, 1.349 & 1.359. From experiment (Fig. 6(b)), the positions of the corresponding transmission dip wavelengths are at 1546nm, 1568.3nm & 1578.8nm respectively. Thus dip wavelength shifts by 22.3 nm & 10.5 nm when sensing r.i. changes by 0.019 and 0.01 respectively giving a sensitivity of 1146.63 nm per RIU. However, as predicted from equation (2) and from simulation (Fig. 6(a)), the corresponding shifts should be 22.135nm & 11.65nm respectively with a sensitivity of 1165nm per RIU. This deviation may be due to the error in measurement of r.i. and/or due to some variation in periodicity and depth of the grating during fabrication. On the other hand, if we would have considered the reference sensing medium as air ($n = 1$) and optimized our grating structure for a period Λ_x = 1550 nm, then the sensitivity would have been 1550nm per RIU (eq.2). From Fig. 6, it can be seen that, in addition to the dip at 1550nm there is another dip at 1610 nm. This dip is due to the phenomenon of GMR effect in the structure whose sensitivity is very less compared to the dip at 1550nm.

In conclusion, we have demonstrated a new technique to sense r.i. based on the principle of simple diffraction in a phase grating. The sensitivity of our proposed sensor comes out to be much higher than other grating based sensors like GMR, LSPR etc. From equation (2), the sensitivity is of the order of the period of the grating. In case of EF sensors, the sensing wavelength does not change directly due to the change in r.i. of sensing medium, rather it is actually a function of the effective index (n_{eff}) of guided mode in the waveguide [12]. This effective index change Δn_{eff}, caused due to r.i. change of sensing medium is very less. For example as in [12], the effective index change Δn_{eff} is only 0.08 when $\Delta n = 1$ which gives a sensitivity of 110 nm per RIU. On the other hand, for our sensor the wavelength shift $\Delta\lambda$ bears a direct relation with Δn governed by Eq. (2), leading to much more sensitivity compared to EF sensors.

References

1. J. Homola, S. S. Yee, and G. Gauglitz, Sens. Act. B **54**, 3(1999).
2. Prasad, P. N. Introduction to Biophotonics (Wiley-Interscience, 2003).
3. K. M. Mayer and J. H. Hafner, Chemical Reviews **111**, 3828 (2011).
4. J. N. Anker, W. P. Hall, O Lyandres, N. C. Shah, J. Jhao, R.P. Duyne, Nature Mater. **7**, 442 (2008).
5. P. K. Jain, M.A. El-Sayed, Nano Lett. **8**, 4347 (2008).
6. S. Nishiuma, Y. Handa, T. Imamura, M. Ogino, Jpn. J. Appl. Phys. **47**, 1828 (2008).
7. W. J. Galush, S. A. Shelby, M. J. Mulvihill, A. Tao, P. Yang, J. T. Groves, Nano Lett. **9**, 2077 (2009).
8. H. Jiang, J. Sabarinathan, J. Phys. Chem. C. **114**, 15243 (2010).
9. A. Densmore, D.-X. Xu, P. Waldron, S. Janz, P. Cheben, J. Lapointe, A. Delâge, B. Lamontagne, J. H. Schmid, and E. Post, IEEE Photon. Technol. Lett. **18**, 2520 (2006).
10. R. Magnusson, Y. Ding, K. J. Lee, P. S. Priambodo & D. Wawro, Proc. Soc. Photo-Opt. Instrum. Eng. **6008**, 1 (2005).
11. J. J. Wang, L. Chen, S. Kwan, F. Liu, X. Deng, J. Vac. Sci.Technol. B **23**, 3006 (2005).
12. J. H. Schmid, W. Sinclair, J. García, S. Janz, J. Lapointe, D. Poitras, Y. Li, T. Mischki, G. Lopinski, P. Cheben, A. Delâge, A. Densmore, P. Waldron, and D.-X. Xu, Opt. Express **17**, 18371 (2009).
13. Q Wang, D Zhang, H Yang, C Tao, Y Huang, S Zhuang and T Mei, Sensors **12**, 9791 (2012).
14. A. Liu, W. H. E. Hofmann, and D. H. Bimberg, IEEE J. Quantum Electron, **51,** (2015).
15. J. W. Goodman, Introduction to Fourier Optics (Third Edition, Roberts & Company, 2007) p.464.
16. Lumerical Solutions, Inc. http://www.lumerical.com/tcad-products/fdtd/
17. M. Sedlatschek, J. Trumpfheller, J. Hartmann, M. Müller, C. Denz, T. Tschudi, Appl. Phys. B **9**, 1047 (1999).
18. P. Günter, Phys. Rep. **93**, 199 (1982).
19. M. Born and E. Wolf, Principles of Optics, 7th ed. (1999), pp.472 and 498.
20. E Hecht and A.R. Ganesan, Optics, 4th ed. (Pearson), p.584.

Fifth page full reference

1. J. Homola, S. S. Yee, and G. Gauglitz, "Surface Plasmon resonance sensors: review," Sens. Act. B 54, 3-15(1999).
2. P. N. Prasad, Introduction to Biophotonics (Wiley-Interscience, 2003).
3. K. M. Mayer and J. H. Hafner, "Localized Surface Plasmon Resonance Sensors," Chemical Reviews 111, 3828-3857 (2011).
4. J. N. Anker, W. P. Hall, O Lyandres, N. C. Shah, J. Jhao, R.P. Duyne, "Bio sensing with plasmonic nanosensors," Nature Mater. 7, 442-453 (2008).
5. P. K. Jain, M.A. El-Sayed, "Noble Metal Nanoparticle Pairs: Effect of Medium for Enhanced Nanosensing," Nano Lett. 8, 4347-4352 (2008).
6. S. Nishiuma, Y. Handa, T. Imamura, M. Ogino, "Localized Surface Plasmon Resonant Metal Nanostructures as Refractive Index Sensors," Jpn. J. Appl. Phys. 47, 1828-1832 (2008).
7. W. J. Galush, S. A. Shelby, M. J. Mulvihill, A. Tao, P. Yang, J. T. Groves, "A Nanocube Plasmonic Sensor for Molecular Binding on Membrane Surfaces," Nano Lett. 9, 2077-2082 (2009).
8. H. Jiang, J. Sabarinathan, "Effects of Coherent Interactions on the Sensing Characteristics of Near-Infrared Gold Nanorings," J. Phys. Chem. C. 114, 15243-15250 (2010).
9. A. Densmore, D.-X. Xu, P. Waldron, S. Janz, P. Cheben, J. Lapointe, A. Delâge, B. Lamontagne, J. H. Schmid, and E. Post, "A Silicon-on-Insulator Photonic Wire Based Evanescent Field Sensor," IEEE Photon. Technol. Lett. 18, 2520-2522 (2006).
10. R. Magnusson, Y. Ding, K. J. Lee, P. S. Priambodo & D. Wawro, "Characteristics of resonant leaky-mode biosensors," Proc. Soc. Photo-Opt. Instrum. Eng. 6008, 1 (2005).
11. J. J. Wang, L. Chen, S. Kwan, F. Liu, X. Deng," Resonant grating filters as refractive index sensors for chemical and biological detections," J. Vac. Sci.Technol. B 23, 3006-3010 (2005).
12. J. H. Schmid, W. Sinclair, J. García, S. Janz, J. Lapointe, D. Poitras, Y. Li, T. Mischki, G. Lopinski, P. Cheben, A. Delâge, A. Densmore, P. Waldron, and D.-X. Xu, "Silicon-on-insulator guided mode resonant grating for evanescent field molecular sensing," Opt. Express 17, 18371-18380 (2009).
13. Q Wang, D Zhang, H Yang, C Tao, Y Huang, S Zhuang and T Mei, "Sensitivity of a Label-Free Guided-Mode Resonant Optical Biosensor with Different Modes Sensors," 12, 9791-9799 (2012).
14. A. Liu, W. H. E. Hofmann, and D. H. Bimberg, "Integrated High-Contrast-Grating Optical Sensor Using Guided Mode," IEEE J. Quantum Electron, 51, (2015).
15. J. W. Goodman, Introduction to Fourier Optics (Indian Edition, Roberts & Company, Colardo, 2007) p.464.
16. Lumerical Solutions, Inc. http://www.lumerical.com/tcad-products/fdtd/
17. M. Sedlatschek, J. Trumpfheller, J. Hartmann, M. Müller, C. Denz, T. Tschudi, "Differentiation and subtraction of amplitude and phase images using a photorefractive novelty filter," Appl. Phys. B 9, 1047-1054 (1999).
18. P. Günter, "Holography, coherent light amplification and optical phase conjugation with photorefractive materials," Phys. Rep. 93, 199-299 (1982).
19. M. Born and E. Wolf, Principles of Optics, 7th ed. (1999), pp.472 and 498.
20. E Hecht and A.R. Ganesan, Optics, 4th ed. (Pearson), p.584.